HF radar polar patch and its relation with the cusp during B_Y-dominated IMF: Simultaneous observations at two altitudes

S. Taguchi,[1] K. Hosokawa,[1] A. Nakao,[1] M. R. Collier,[2] T. E. Moore,[2] N. Sato,[3] and A. S. Yukimatu[3]

Received 20 July 2008; revised 3 October 2008; accepted 9 December 2008; published 20 February 2009.

[1] Recent studies have shown that the motion of the cusp can be deduced from the energetic neutral atom signals detected in the magnetosphere by the Low Energy Neutral Atom (LENA) imager on the IMAGE spacecraft. We use this approach to understand the characteristics of the formation of a polar patch seen in the dayside ionosphere. During a period of the 28 March 2001 LENA cusp signal event, the SuperDARN radars at Syowa East, Syowa South, and Kerguelen Island identified large-scale features of a polar patch. A region of high backscatter power observed by the radars separates into two parts around 77°, and its high-latitude part moves in the poleward and duskward direction. The separation latitude is about 5° higher than the equatorward boundary of the cusp, which is deduced from the LENA cusp signal. We interpret these observations, including features obtained with other SuperDARN radars in the northern hemisphere, as being due to the IMF B_Y-controlled zonal jet flow that occurred during a period of increase in $|B_Y/B_Z|$, without requiring the change in B_Y polarity that has been often invoked in previous studies. The sharp equatorward boundary of the radar signatures of the polar patch would be an interface between the preexisting flow generally in the antisunward direction and the enhanced zonal flow. The flow enhancement appears to be a fundamental process that forms the large-scale polar patch at latitudes several degrees higher than the cusp.

Citation: Taguchi, S., K. Hosokawa, A. Nakao, M. R. Collier, T. E. Moore, N. Sato, and A. S. Yukimatu (2009), HF radar polar patch and its relation with the cusp during B_Y-dominated IMF: Simultaneous observations at two altitudes, *J. Geophys. Res.*, *114*, A02311, doi:10.1029/2008JA013624.

1. Introduction

[2] The low-altitude cusp is the site that reflects the magnetospheric phenomena most directly controlled by the solar wind and interplanetary magnetic field (IMF). When the southward component of IMF increases, the low-altitude cusp, which is defined by the magnetosheath particle precipitation, shifts equatorward [e.g., *Burch*, 1973; *Newell et al.*, 1989]. Magnetosheath particle entry into the high-altitude cusp is caused by reconnection and occurs in a latitudinally narrow region. This spatially limited source, operating on the antisunward flow of the magnetic flux tube during southward IMF, causes ion dispersion signature in which the average ion energy decreases with increasing latitude at the low-altitude cusp [*Reiff et al.*, 1977]. This ion dispersion is one of the well-known signatures from which we can deduce the magnetospheric phenomena directly controlled by the solar wind and IMF [e.g., *Menietti and Burch*, 1988; *Lockwood and Smith*, 1992; *Escoubet et al.*, 1992; *Onsager et al.*, 1993; *Taguchi et al.*, 1993; *Newell and Meng*, 1994; *Yamauchi et al.*, 1995; *Lockwood et al.*, 1998; *Bosqued et al.*, 2005; *Trattner et al.*, 2005].

[3] The low-altitude cusp also shows prominent signatures as a result of the interaction between the strongly eastward/westward IMF and the magnetosphere. For the eastward (or westward) IMF, i.e., positive (or negative) IMF B_Y, a strong westward (or eastward) flow appears in the low-altitude cusp of the northern hemisphere [e.g., *Heppner*, 1972; *Mozer et al.*, 1974; *Heelis*, 1984]. The pattern in the southern hemisphere is generally a mirror image of the northern pattern with respect to the noon-midnight meridian [e.g., *Heppner*, 1972]. These asymmetries in the low-altitude cusp are an indication of the magnetic tension force acting on reconnected magnetic field lines [e.g., *Cowley et al.*, 1991]. Besides the convection distribution, the low-altitude cusp also shows the B_Y-controlled distribution of the field-aligned current, which can be also interpreted in terms of the reconnection [e.g., *Taguchi et al.*, 1993; *Farrugia et al.*, 2003].

[4] When IMF is northward, the low-latitude cusp shows intriguing features. A field-aligned current with polarity reversed with respect to the one for the Region 1 current appears in the poleward part of the cusp [e.g., *Araki et al.*, 1984; *Iijima et al.*, 1984]. The convection also shows a reversed polarity in that region [e.g., *Burke et al.*, 1979; *Reiff*, 1982; *Matsuoka et al.*, 1996; *Taguchi and Hoffman*, 1996]. The ion dispersion also shows a reversed type [e.g.,

[1]Department of Information and Communication Engineering, University of Electro-Communications, Tokyo, Japan.
[2]NASA Goddard Space Flight Center, Greenbelt, Maryland, USA.
[3]National Institute of Polar Research, Tokyo, Japan.

Copyright 2009 by the American Geophysical Union.
0148-0227/09/2008JA013624

Burch et al., 1980; *Basinska et al.*, 1992]. All these phenomena can be associated with the reconnection poleward of the cusp.

[5] Irrespective of IMF orientation, the quasi-steady phenomena seen in the low-altitude cusp appear to be well understood in terms of reconnection. However, when we advance our study of the IMF control of the phenomena having a timescale of several minutes, it is difficult to determine whether or not the phenomena is related to the variation in IMF observed upstream in the solar wind, because of the timing uncertainty of the solar wind propagation from the upstream spacecraft position to the dayside magnetopause. *Collier et al.* [1998] have studied the timing accuracy extensively using WIND and IMP 8 magnetometer data, and shown that large timing uncertainties exist in the solar wind convection.

[6] Recently, a remote sensing approach has been presented which can avoid the timing uncertainty, i.e., monitoring the high-altitude cusp motion with energetic neutral atoms (ENAs) [*Taguchi et al.*, 2004a, 2004b, 2005, 2006a, 2006b; *Murata et al.*, 2007]. These authors have shown that the ENA signals in the direction of the high-latitude magnetopause (detected by the Low Energy Neutral Atom (LENA) imager [*Moore et al.*, 2000] on the IMAGE spacecraft), reflect the motion of the high-altitude cusp, extending the finding that ENAs detected by LENA in the magnetosphere include the result of solar wind ions charge-exchanging with the hydrogen exosphere in the magnetosheath flow [*Collier et al.*, 2001a, 2001b; *Fok et al.*, 2003; *Moore et al.*, 2003].

[7] In this paper we use this remote sensing approach to understand the characteristics of the formation of the poleward propagating backscatter features seen by HF radar near the low-altitude cusp. These features have been identified as the HF radar signatures of polar patches, i.e., regions of plasma density enhanced above a lower background level and propagating generally in the antisunward direction [e.g., *Buchau et al.*, 1983; *Weber et al.*, 1984; *Anderson et al.*, 1988; *Pinnock et al.*, 1993; *Valladares et al.*, 1994; *Rodger et al.*, 1994; *Ogawa et al.*, 1998, 2001; *Rodger and Rosenberg*, 1999; *Milan et al.*, 2002]. Results from a case study based on coordinated observations in the high- and low-altitude cusp are presented.

[8] On 28 March 2001, large-scale polar patch features were identified by three SuperDARN radars [*Greenwald et al.*, 1995] in the southern hemisphere. Around the time of the polar patch formation IMAGE/LENA observed the start of the poleward motion of the cusp signal in the northern hemisphere. The footprint of the LENA cusp signal is about 5° lower than the latitude of the polar patch separation, suggesting that cusp particle precipitation is not the magnetospheric counterpart of the polar patch for this event.

[9] Near the footprint of the LENA cusp signal, a strong westward flow with a sunward component was identified by the SuperDARN radars in the northern hemisphere. This is consistent with previous observations showing that the polar patch formation occurs within a few minutes of a short-lived plasma jet [e.g., *Pinnock et al.*, 1993; *Valladares et al.*, 1994; *Rodger et al.*, 1994; *Milan et al.*, 2002]. In our event, however, the IMF change reported in previous studies, i.e., IMF B_Y polarity change or B_Y change to near zero, is not identified; rather, our study indicates that the increase in $|B_Y/B_Z|$ is important. We interpret all observations in this event as being due to the enhancement of the IMF B_Y-controlled zonal flow after a period of more southward IMF.

2. Previous Research on the Changes in IMF for Polar Patch Formation

[10] Several mechanisms have been proposed to explain the formation of the polar patches. We summarize those studies here into four categories only in terms of the association of the changes in IMF, putting aside discussion of their generation mechanisms until section 4.

[11] The first category is the increase of negative B_Z and the subsequent less negative (or positive) B_Z, which is expected to cause the sudden expansion and then contraction of the convection pattern near the cusp [e.g., *Anderson et al.*, 1988; *Lockwood and Carlson*, 1992]. When the convection pattern contracts, the high-density plasma, which was transported from the sunlit ionosphere, becomes isolated, forming a polar patch. The second category is the change from positive B_Z to negative B_Z. This may initiate a poleward motion of the isolated high-density plasma [e.g., *Valladares et al.*, 1998; *MacDougall and Jayachandran*, 2007]. The third one is the changes in the polarity of the IMF B_Y component [e.g., *Sojka et al.*, 1993; *Milan et al.*, 2002]. The tongue of the ionization is broken into patches as the convection throat moves in response to B_Y polarity change. The final category is the change in the B_Y polarity or the change to near zero from a significant value of B_Y concurrent with the southward turning of IMF [e.g., *Rodger et al.*, 1994; *Oksavik et al.*, 2006]. The polar patch forms during the interval of the significant B_Y component, and then begins to progress poleward, responding to $B_Y \sim 0$. As will be shown later, the event shown in this paper does not fall into any of these four categories.

3. Observations

3.1. Poleward Propagating Backscatter Features in the Southern Ionosphere

[12] The SuperDARN radars at Syowa East, Syowa South (~69°S, ~40°E for both), and Kerguelen Island (49.35°S, 70.26°E) observed poleward propagating backscatter features around 0840 UT on 28 March 2001. Figure 1 show a sequence of four scans from the Syowa East and Syowa South radars around the time of the polar patch formation. The top four plots are backscatter power data from both radars, which show that a polar patch is observed as a separated high power region around 80° in MLAT between 1000 and 1200 in MLT at 0841 UT and 0842 UT. This location is on the sunward side of the day/night terminator.

[13] Before its separation, a whole high power region extended from ~81° to ~73°. The equatorward part (from ~73° to ~77°) does not change so much before or after the patch formation, indicating that it is a persistent feature. These latitudes would overlap with the cusp, considering that the statistical relation of the cusp latitude to IMF B_Z [*Newell et al.*, 1989] gives a cusp of 73°–77° for B_Z of −5 to 0 nT in this event (shown later). Note that the equatorward boundary of the backscatter region does not move equatorward during the course of the polar patch formation, but rather shifts slightly poleward, suggesting that the

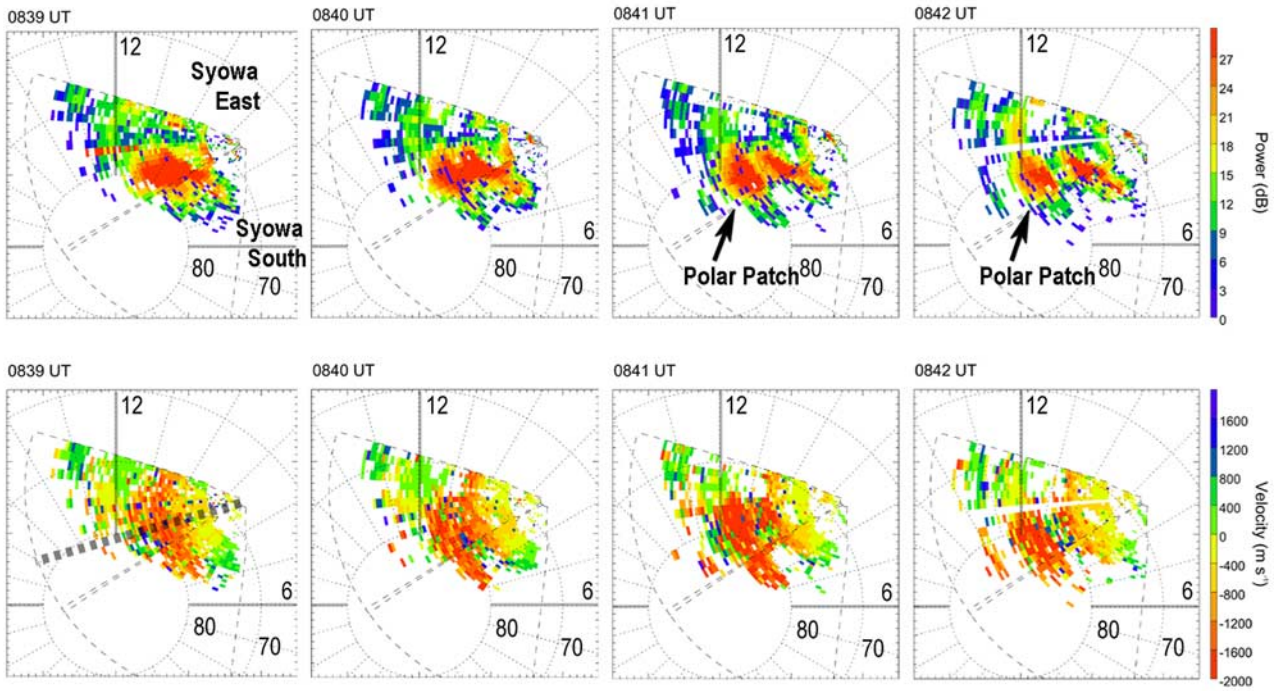

Figure 1. Sequence of four scans from Syowa East and Syowa South radars around the time of the polar patch formation. (top) Backscatter power data and (bottom) the line of sight (LOS) velocity data. The backscatter power data show that a polar patch appears as a separated high-power region around 80° in MLAT between 1000 and 1200 in MLT at 0841 UT and 0842 UT. The magnitude of the LOS velocity of the polar patch exceeds 1.6 km s^{-1}. The thick dashed line in the bottom left (velocity map at 0839 UT) indicates the direction of Beam 4 of the Syowa East radar. Velocity data from this beam will be shown later in Figure 6.

formation of the polar patch is not associated with the southward turning of IMF. Also noticeable in the power data is a sharp boundary of the trailing edges of the patch, as with the event shown in the work of *Milan et al.* [2002].

[14] The bottom plots in Figure 1 show the line of sight (LOS) velocity. Reddish color represents the velocity away from the radar, and the velocity toward the radar is shown with greenish color. The figures at 0841 or 0842 UT show that the LOS velocity of the polar patch exceeds 1.6 km s^{-1}. At 0842 UT the LOS velocities behind the polar patch (77°–80° in 0900–1100 MLT) take rather scattered values (both positive and negative values), and it is difficult to deduce a convection pattern with only these data. For this region (which is also the low backscatter power region in Figure 1, top), the radar at Kerguelen Island, located near noon at this time, observed a relatively stable direction of flow. Figure 2 shows the LOS velocity at 0842 UT. The ellipse in the figure represents the crude location where the Syowa East and South radars received very low backscatter signals. The LOS velocities in this region have a component toward the radar, i.e., a sunward component.

[15] In Figure 2, at higher latitudes between 1000 and 1400 MLT there is a region having an antisunward flow component. The prenoon part of this region overlaps with the high power region identified as the polar patch in Figure 1, suggesting that motion of the polar patch has an antisunward flow component as well as a duskward component. This indicates that the polar patch is entrained with the

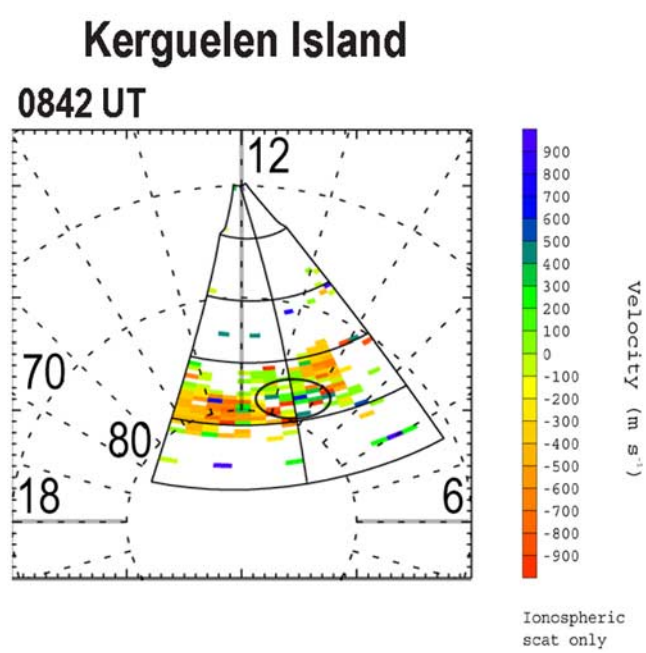

Figure 2. LOS velocity data from the Kerguelen Island radar at 0842 UT. The ellipse represents the crude location of the region from which the Syowa East and South radars observed very low backscatter power. The flow has a sunward component in this region (bluish/greenish color).

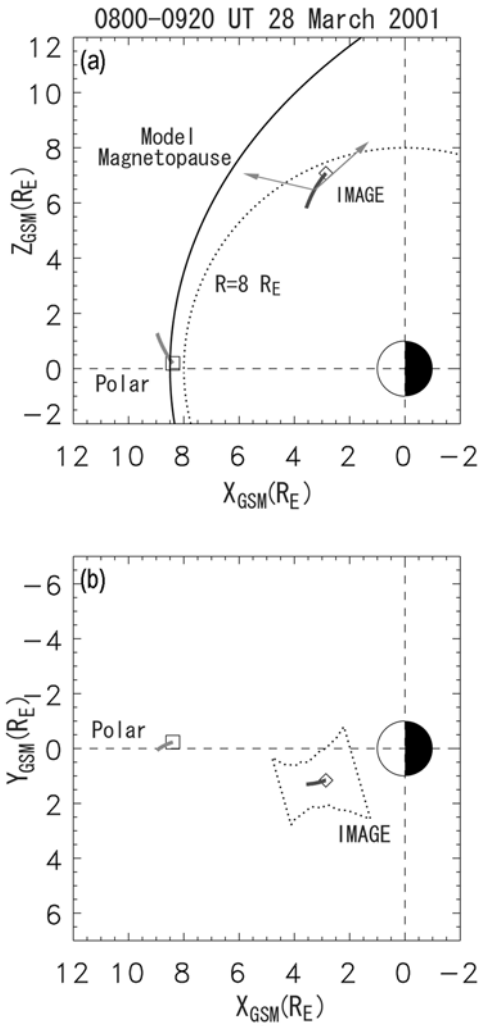

Figure 3. Position of IMAGE and Polar in (a) X_{GSM}-Z_{GSM} (b) X_{GSM}-Y_{GSM} planes for 28 March 2001, 0800–0920 UT. The diamond and square indicate the location of the spacecraft at 0800 UT. Two arrows from the IMAGE location at ~0840 UT in Figure 3a represents a 136° field of view of LENA that is used for our analysis. The dotted curve in Figure 3a shows the radial distance of 8 R_E from the center of the Earth, and the outermost solid curve represents the magnetopause predicted by *Shue et al.* [1998]. The region shown surrounded with dots in Figure 3b represents the 136°FOV of LENA which is mapped on the sphere with a radius of 8 R_E.

convection for negative IMF B_Z. This will be discussed later.

3.2. High-Altitude Cusp and Solar Wind

[16] During more than 1 h including ~10 min for polar patch observation, LENA/IMAGE observed an enhanced ENA signal from the high-altitude cusp. The emission of ENAs is produced by the charge-exchange of ions with the hydrogen exosphere. The flux of the ENAs detected by the instrument can be expressed as the LOS integration of the product of the source ion flux and the hydrogen exospheric density [e.g., *Roelof and Skinner*, 2000]. The ENAs essentially retain the energy and the direction of the incoming ions, and the detected ENA flux is proportional to the source ion flux.

[17] Figures 3a and 3b show the orbit of IMAGE in the X_{GSM}-Z_{GSM} and X_{GSM}-Y_{GSM} planes for the interval that we analyzed in this paper, respectively. IMAGE is located near (X_{GSM}, Z_{GSM}) = (~3 R_E, 6–7 R_E) in the postnoon sector (Y_{GSM} ~ 1 R_E). During this event Polar is located near the subsolar magnetopause. We include the orbit of Polar in Figures 3a and 3b. The Polar magnetic field experiment (MFE) [*Russell et al.*, 1995] observed IMF in the magnetosheath, which will be shown later. Polar exited to the magnetosheath at ~0804 UT, after crossing the magnetopause at X_{GSM} ~ 8.5 R_E. In Figure 3a, the outermost solid curve represents the possible shape of the magnetopause with the subsolar distance of 8.5 R_E. We used an IMF B_Z of −2 nT and a dynamic pressure of 6 nPa as inputs to the model by *Shue et al.* [1998].

[18] The LENA imager on IMAGE detects ENAs arriving at the spacecraft from within a 90° field of view, swept through 360° every 2 min by a spacecraft spin with a vector antialigned with the orbital angular momentum vector [*Moore et al.*, 2000]. Two gray arrows from the midpoint on the IMAGE orbit in Figure 3a indicate the approximate projection of a 136° (=17 spin angle sectors) field of view (FOV) out of 360° to the Y_{GSM} = 0 meridian at 0840 UT. We focused on the LENA count data in this range, which covers the direction of the cusp while excluding the "Sun signal," which is produced primarily by the charge exchange of solar wind protons prior to becoming slowed and heated across the bow shock [*Collier et al.*, 2001a, 2001b, 2003]. Note that this range looks into the higher latitudes than that for an event during large negative IMF B_Z on 11 April 2001 in the work of *Murata et al.* [2007] (their Figure 1). In our event, the LENA may miss the cusp signal if B_Z becomes very negative. This will be discussed later.

[19] In Figure 3b, the region surrounded by dots indicates the FOV of LENA, which is mapped on the sphere with a radius of 8 R_E. The region inside this distorted boundary is somewhat narrow near X_{GSM} ~ 3 R_E compared with the smaller and larger X_{GSM} parts. This simply reflects that the mapping surface for the FOV in the middle part is close to the location of the spacecraft (Figure 3a).

[20] Figure 4 shows variations of LENA hydrogen count rate in the 17 sectors (defined above), together with ACE solar wind, and Polar magnetic field in the magnetosheath. For the comparison of the LENA data, the Polar and ACE data are delayed by 4 min and 40 min relative to the IMAGE observations, respectively. Throughout the plotted interval the solar wind speed is relatively constant at ~650 km/s (Figure 4a). The solar wind number density varies from 5 cm^{-3} to 15 cm^{-3} (Figure 4b). Because of the enhanced density plus the relatively high solar wind speed, the solar wind dynamic pressure (Figure 4c) is also relatively high (~4 nPa to ~11 nPa). The dynamic pressure is calculated from the speed (Figure 4a) and density (Figure 4b) assuming 4% He^{++} particles.

[21] In the first half of the plotted interval ACE IMF B_Y (blue in Figure 4d) is strongly positive, and the dominant component. The IMF B_Z component (red in Figure 4d) varies mostly between ±7 nT. In the latter half, B_Z becomes more negative, decreasing the B_Y component, and then IMF becomes strongly northward at the end of the plotted

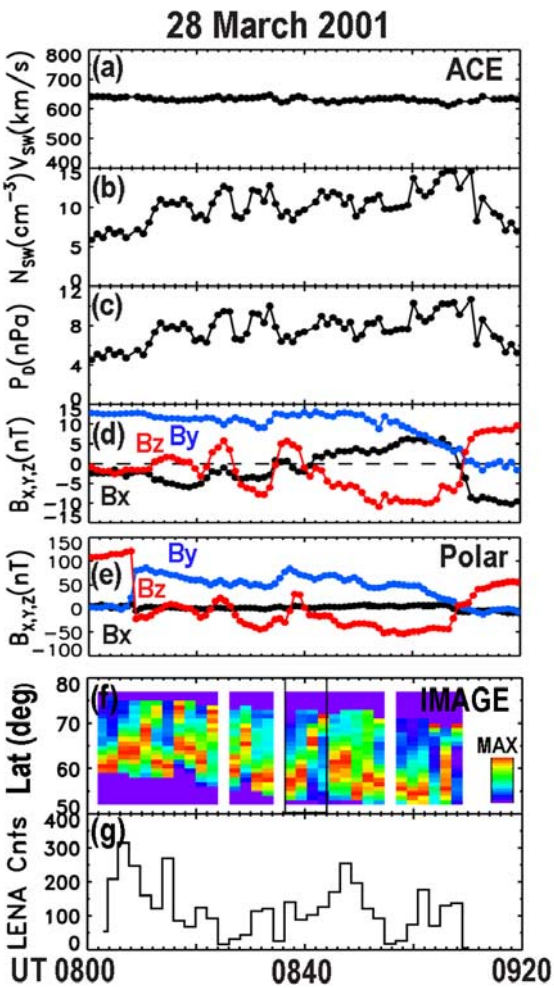

Figure 4. (a) ACE plasma velocity, (b) number density, (c) dynamic pressure, (d) three components of IMF in GSM, (e) Polar magnetic field, (f) LENA spectrogram, and (g) LENA count. In Figure 4d 64-s averages of IMF data that were created from original 16-s averages are plotted so as to make comparison between the IMF and plasma data easier. The vertical axis of Figure 4f represents the latitude of the emission mapped on the sphere of 8 R_E, not the magnetic latitude. In Figure 4f the normalized values are plotted so that the maximum peak can be unity in each time. Reddish color represents larger counts. The two vertical lines represents 10 min interval around the time of polar patch formation, which was identified in Figure 1.

interval. Figure 4e shows Polar magnetic field data. In the beginning of the plotted interval, Polar was in the magnetosphere and exited the magnetosheath several minutes later. The Polar magnetic field variations in the sheath have a correlation with the ACE magnetic field variations (Figure 4d). From this correlation we chose 36 min (=40 min−4 min) as the solar wind convection time from ACE to Polar.

[22] Figure 4f shows the variations of the direction of the LENA cusp signal. We introduce a sphere of 8 R_E as a "screen" [*Taguchi et al.*, 2005] to monitor the source ions for the LENA cusp signal, which are thought to be located somewhere between the satellite position and the magnetopause (see Figure 3a). The vertical axis of Figure 4f represents the latitude of the LENA emission mapped on the screen. The hydrogen background corrected scaled count rate was averaged in a moving (by 1° step) 5° window of latitude [*Murata et al.*, 2007] except for the time when the total count (shown in Figure 4g) is very small (defined as less than 25 counts), and the normalized values were plotted so that the maximum peak can be unity in each time. The two vertical lines represent 8 min intervals around the polar patch formation.

[23] Comparison between Figures 4e and 4f shows that the location of the LENA cusp signal responds to IMF B_Z variations [*Taguchi et al.*, 2004a, 2004b, 2005; *Murata et al.*, 2007]. The latitude tends to be low when B_Z is more negative. In this case, the B_Y component is stronger than B_Z until ~0850 UT, which means that the relatively small tilting of the dominantly duskward IMF causes the motion of the LENA cusp signal. Around the polar patch formation the LENA cusp signal moves poleward from the relatively low latitude (0837–0843 UT). Note that the LENA count at 0835 UT is very low (Figure 4g). This will be discussed later.

3.3. Plasma Flow in the Ionosphere

[24] Figure 5 shows the LENA snapshots at 0837 UT and the plasma flow obtained with SuperDARN radars in the northern ionosphere immediately before the polar patch formation. In the LENA snapshot (top of Figure 5), the hydrogen count rate for each line of sight (for 136°FOV defined in Figure 3) is plotted on the sphere with a radius of 8 R_E. The purple color represents the region having a relatively high count, which is defined as ≥4 counts. The lowest-latitude point of this region is located approximately at (X_{GSM}, Y_{GSM}, Z_{GSM}) = (4.4, 1.3, 6.6) R_E, and the highest latitude point is at (X_{GSM}, Y_{GSM}, Z_{GSM}) ~ (3.9, 1.2, 6.9) R_E.

[25] These two points are mapped to the ionosphere. These footprints are shown with two open squares in Figure 5 (middle and bottom). Figure 5 (middle and bottom) also shows LOS velocities obtained with the SuperDARN radars at Hankasalmi, Finland (63.32°N, 26.61°E) and Pykkvybaer, Iceland (63.86°N, 19.20°E), respectively. For the mapping, we used the Tsyganenko 96 model with inputs of (B_Y, B_Z) = (13, 0) nT, P_{dyn} = 10 nPa, and Dst = −30 nT, although the input of the IMF B_Y (13 nT) for the Tsyganenko 96 model is beyond the range of reliable approximation. A time delay of 3 min is considered for comparison between the LENA data and the SuperDARN data. This will be discussed when Figure 7 is shown.

[26] The footprint occurs around 72° MLAT. This latitude is similar to the one for the equatorward boundary of the high backscatter power region in the southern ionosphere (Figure 1). The Hankasalmi data (Figure 5, middle) show that LOS velocities have a sunward component (greenish or bluish color) near the footprint. On the prenoon side the LOS velocities have an antisunward component (reddish color). The spectral widths near the equatorward boundary of these flow regions are very broad, above 400 ms^{-1}. The backscatter region represents a part of the cusp [e.g., *Baker et al.*, 1995; *Hosokawa et al.*, 2002]. The Pykkvybaer radar data (Figure 5, bottom) indicate that the flow also has a strong dawnward component, which is typical for positive IMF B_Y in the northern hemisphere.

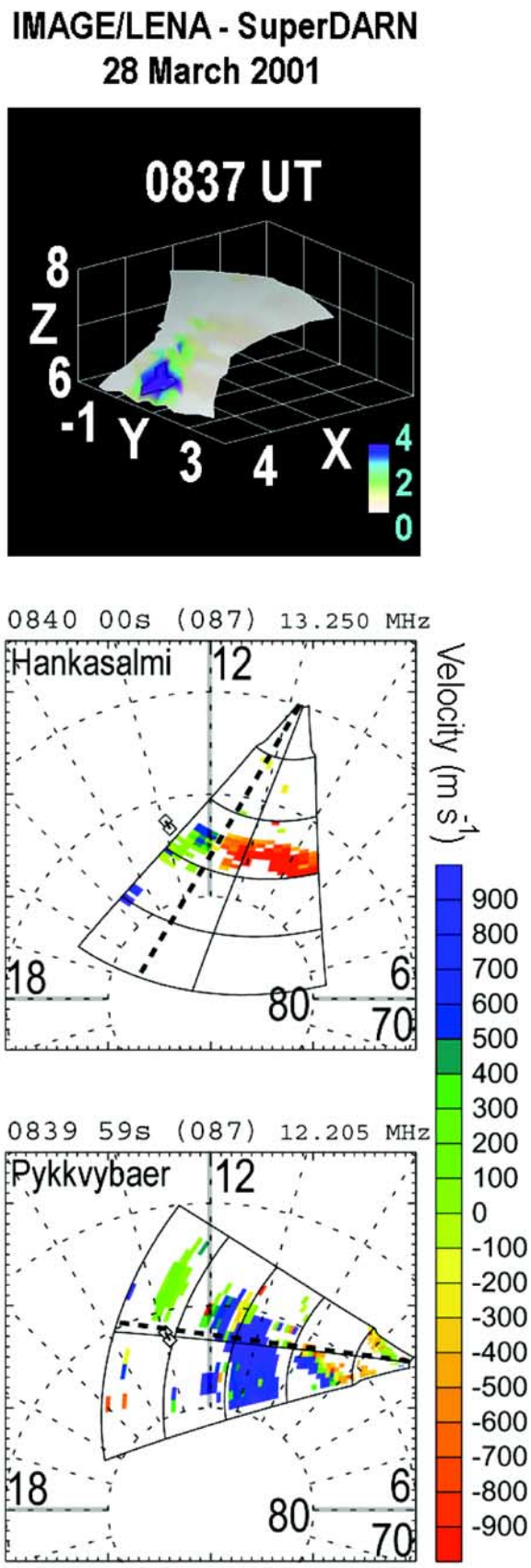

Figure 5. (top) LENA snapshots plotted on the sphere with a radius of 8 R_E and (bottom) spatial maps of the LOS velocity from Hankasalmi and Pykkvybaer radars immediately before polar patch formation. In the LENA snapshot the purple color represents the region having a relatively high count, which is defined as >4 counts. Two open squares in the velocity maps indicate the footprint of this high count region. The dashed lines in the maps of the LOS velocity from the Hankasalmi and Pkkkvybaer radars represent Beam 11 and Beam 8, respectively. Data from these beams will be shown in Figure 6.

[27] How the LOS velocities from these two radars and the direction of the LENA cusp signal change during the course of the polar patch formation is shown in Figure 6. Figure 6a shows the LENA spectrogram, and Figures 6b–6d are the LOS velocity plots from the Pykkvybaer, Hankasalmi, and Syowa East radars in the range gate versus UT format. Time delay of the SuperDARN data from the LENA data is not included in this figure. A polar patch can be identified as poleward propagating backscatter features in the data from the Syowa East radar (Figure 6d), as has been identified in previous studies [e.g., *Pinnock et al.*, 1993; *Rodger et al.*, 1994; *Ogawa et al.*, 1998; *Nishitani et al.*, 1999; *Milan et al.*, 2002]. A dashed line indicates the time (0841 UT) for the polar patch formation, which was determined in Figure 1.

[28] Figure 6b (beam 8 of the Pikkvybaer radar) shows that the LOS velocities toward the radar (bluish color) start to increase 3–4 min before the polar patch formation. The flow direction is dawnward, and the flow magnitude exceeds 1.6 km s^{-1}. Data from beam 11 of the Hankasalmi radar (Figure 6c) indicate that the flow has an antisunward component or sunward component before or after the dashed line, respectively. We will show that this change contains spatial effect later. Since the FOV of these two beams intersect near noon (Figure 5), we know from these observations that the plasmas flow in the antisunward and westward direction before the polar patch formation and that the polar parch forms when the zonal flow component is enhanced.

[29] Data from the Hankasalmi radar also show that the equatorward boundary of the backscatter region, which would be inside the cusp, is located at ~74° MLAT (vertical axis on the right-hand side) before the time of the polar patch formation. This boundary starts to move poleward 3–4 min before the polar patch formation. Considering that this boundary is at relatively low latitudes around that time, the very low LENA count at 0835 UT implies that the cusp is located at lower latitudes than the LENA's FOV at this time.

[30] Both the LENA and Hankasalmi radar data show that the cusp is moving poleward when the polar patch appears. As is expected from this poleward motion, a trend of decreasing negative B_Z can be identified during the corresponding interval of the Polar magnetic field data (Figure 4e) although B_Z takes a positive value during a brief interval, ~2 min. The decrease in negative B_Z increases $|B_Y/B_Z|$ during a period of relatively constant B_Y. This would produce the zonal flow in the ionosphere.

[31] How the spatial distribution of the LOS velocities observed by these three radars, plus the Kerguelen radar,

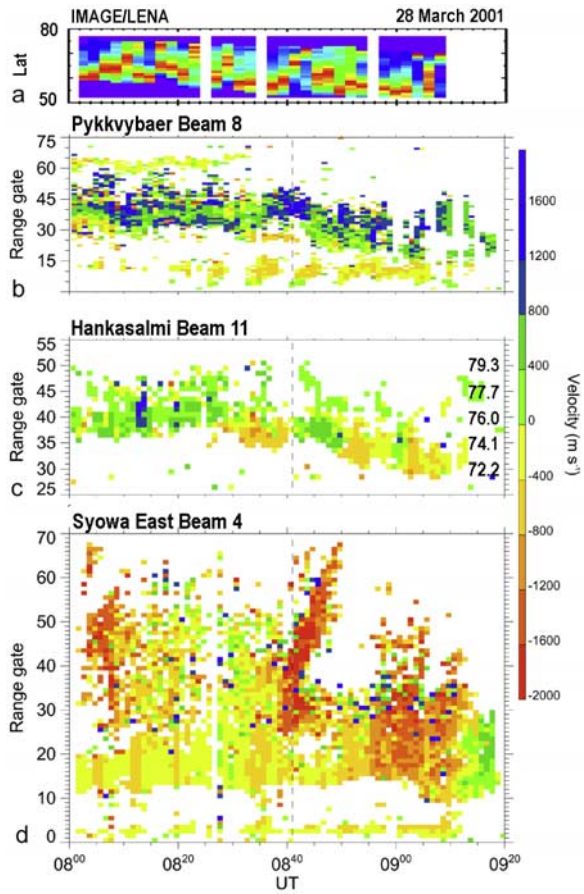

Figure 6. (a–d) LENA spectrogram and LOS velocity plots from the Pykkvybaer, Hankasalmi, and Syowa East radars during 0800–0920 UT. A polar patch can be identified as poleward propagating backscatter features in the data from the Syowa East radar (Figure 6d). A dashed line indicates the time (0841 UT) for polar patch formation. Beam 8 of the Pykkvybaer radar (Figure 6b) is near the center of the FOV (see Figure 5, bottom), and Beam 11 of the Hankasalmi radar (Figure 6c) is in the eastward part of the FOV (see Figure 5, middle). Magnetic latitude is shown along the right vertical axis of the plot of the Hankasalmi data. Time delay of the SuperDARN data from the LENA data is not included in this plot.

changes after the polar patch formation is shown in Figure 7 together with corresponding LENA snapshots. The LOS velocity data from Hankasalmi at 0840 UT show that the boundary between the sunward and antisunward flow regions exists near 1200 MLT. After that, the boundary moves toward the prenoon side so that the region having a sunward component can occupy in a larger area near noon. This motion can be seen at beam 11 (Figure 6c) as the flow change from an antisunward direction (reddish color) to a sunward direction (greenish color). The Hankasalmi radar data in Figure 7 also show that the boundary reaches near 1100 MLT at 0846 UT and then starts to return toward the original MLT.

[32] The LENA cusp moves poleward until 0843 UT and then returns to lower latitudes. Our choice of 3 min as the time delay is based on this correlation. Most of this delay time would come from the transit time of the flow between the MLT of the flow boundary mentioned above and the MLT of the LENA cusp footprint rather than the transit time of the Alfven wave from the high-altitude cusp to the low-altitude cusp. In an event identified near the footprint of the LENA cusp signal, no time delay is needed to explain the convection [*Murata et al.*, 2007].

[33] The Pykkvybaer data show that the flow has a dawnward component at latitudes roughly up to 80° MLAT in the prenoon sector throughout the plotted interval. Comparison between the data from Syowa East and those from Kerguelen shows that the flow has a sunward component (greenish or bluish color in the Kerguelen data) immediately equatorward of the polar patch throughout the interval. This greenish/bluish region expands toward the dusk. Accordingly, the antisunward flow region near 80° in the Kerguelen data also moves toward the dusk. The westward part of this antisunward flow region overlaps the duskward LOS velocity of the polar patch seen in the Syowa East radar. The polar patch drifts in the antisunward and westward direction.

4. Interpretation and Discussion

4.1. Flow Pattern at the Formation of the Polar Patch

[34] To interpret the observation, we first discuss the flow pattern immediately before the polar patch formation, using the LOS velocity data from the Hankasalmi and Kerguelen radars at 0840 UT (Figure 8). In the northern map (Figure 8a) we show the footprint of the reconnection line at ~72° so that the line may overlap with the footprint of the LENA cusp signal (squares). Since the LENA cusp signal is produced by the injected ions along the reconnected field line, the footprint of the LENA cusp signal should be in a position very close to the footprint of the reconnection line. Solid evidence for this correspondence has been provided in a recent study by *Suzuki et al.* [2008] based on an event of simultaneous observations from LENA and the Far-Ultraviolet Instrument [*Mende et al.*, 2000] on IMAGE. It is important that the latitude of the reconnection line is much lower than the center latitude of the polar patch, i.e., around 80°. Seemingly, both poleward moving features might lead to the interpretation that the poleward motion of the LENA cusp signal is a flux transfer event and that this is the magnetospheric counterpart of the polar patch. However, the large difference in latitudes cannot allow such an interpretation.

[35] In Figure 8a, two reference points are shown on the reconnection line. Point A is determined as a location to which the reconnection line should at least extend eastward. This extension is required to explain the flow toward the radar in the postnoon sector, i.e., greenish color regions at ~75° in ~1300 MLT. The flow from A would be as is indicated with the open arrow. The velocity along the arrow direction as shown produces a small V_{LOS} toward the radar, but the observed V_{LOS} reaches 800 m s^{-1}. This indicates that the actual flow is very fast. For example, when the flow is assumed to make an angle of 75° with the LOS direction, V_{LOS} of 800 m s^{-1} means a flow speed of ~3 km s^{-1}.

[36] On the prenoon side, flow has an antisunward component. Considering that the antisunward component is large (~1 km s^{-1}) near 1000 MLT, such flow would be

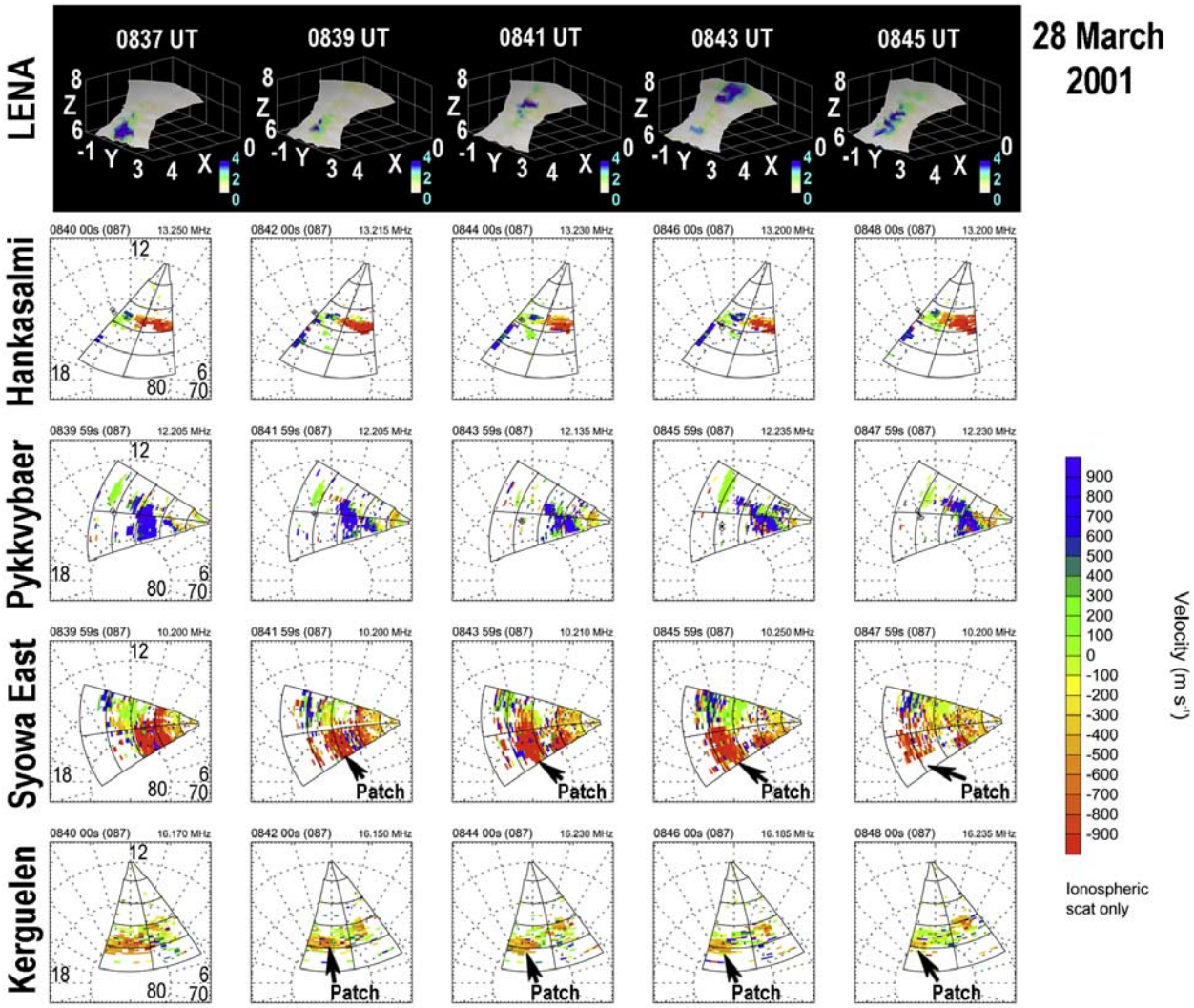

Figure 7. LENA snapshots and LOS velocities measured by the SuperDARN radars at Hankasalmi, Pykkvybaer, Syowa East, and Kerguelen immediately before and after the time of polar patch formation. Format of the LENA snapshot is the same as that of Figure 5.

relatively close to the reconnection line, not in the "old" flux tubes after traveling for a long period of time from the postnoon reconnection site. We assume that the reconnection line extends at least to 1130 MLT (reference point B). At this MLT the boundary between the sunward and antisunward flow regions can be seen. The flow from B should be as is shown with an open arrow, so as to explain the flow having a component away from the radar on the westward side. For simplicity, we have drawn the reconnection line to the westward boundary of the radar's FOV.

[37] In the southern hemisphere map (Figure 8b) we show the reconnection line at the same latitude as the one in the northern hemisphere. Previous studies have shown that the dayside closed field lines have the same sense as the IMF B_Y such that in effect the IMF B_Y field will penetrate the region of closed field lines [*Cowley and Hughes*, 1983; *Crooker et al.*, 1987]. The reconnection line in the southern hemisphere would be then displaced toward the early MLT in this positive IMF B_Y situation. We have flipped over the reconnection line and the possible flow direction with respect to 1100 MLT so that this effect can be incorporated. Two reference points appear at 0830 and 1030 MLT, and we refer to these points as C and D. The ellipse in Figure 8b represents the crude position where the Syowa East and South radars identified the separation of the polar patch at 0841 UT. The flow in this region has a sunward component.

[38] The flow between this region and point D has an antisunward component. This is consistent with the flow direction of the open arrow. No backscatter signals are observed near C, but the data from Syowa South radar (bottom of Figure 1) have shown that there is flow away from the radar, which is also consistent with the direction of the open arrow near C. If the flow extends to higher latitudes as is shown with the arrow, it explains the LOS velocities (bluish color) in the region shown with the ellipse.

[39] In Figure 9, we schematically illustrate the inferred plasma density profile and the flow pattern at the time when the polar patch forms. The plasma density profile (shown with dashed contours) represents that the tongue of ionization

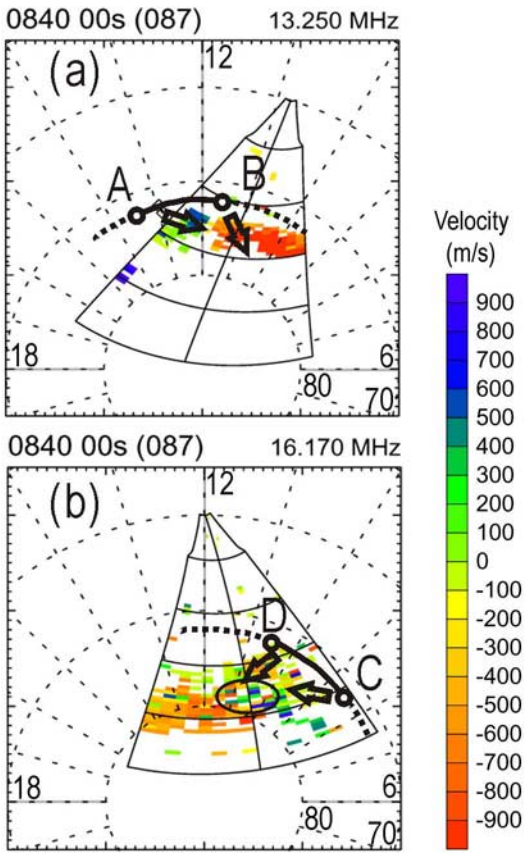

Figure 8. Possible configuration of the footprint of the reconnection line and the flow direction near the (a) northern and (b) southern cusps at 0840 UT, plotted over LOS velocities from the Hankasalmi and Kerguelen radars. The footprint of the reconnection line is drawn at ~72° MLAT so that the line may overlap with the footprint of the LENA cusp signal (squares) determined in Figure 5.

that was created before the polar patch formation is about to be broken into a patch. Faster flow (longer bold arrows) produces less dense plasma in the tongue of the ionization by some mechanism in response to the increase in IMF $|B_Y/B_Z|$, and creates a polar patch. For the less dense plasma, we will test two mechanisms later.

[40] The solid curve represents the footprint of the dawnward extended portion of the reconnection line. This footprint appears in response to the increase in IMF $|B_Y/B_Z|$. Flow emerges from this line as is shown with open arrows. In the magnetosphere, the reconnected flux tube moves sunward and eastward toward the near-noon magnetopause because of the large tension force [e.g., *Gosling et al.*, 1990], overcoming the antisunward sheath flow. Near noon meridian on the magnetopause, the antisunward sheath flow would be small, and the tension force would be relatively strong. The longitudinal flow controlled by the tension force on the dayside magnetopause would be mapped to a latitudinally narrow region in the prenoon sector of the ionosphere, creating the enhanced zonal flow. In this event the center latitude of the zonal flow is ~77° (Figure 2). This latitude appears to be typical as the maximum of the flow speed, i.e., electric field, or the equivalent magnetic perturbation for the cusp during $|B_Y| \gg |B_Z|$ condition [*Taguchi et al.*, 1993].

[41] Shorter bold arrows indicate the flow direction of the polar patch. This has a poleward component because the flux tube in this region reconnected with more southward IMF. Dots behind the shorter bold arrows represent the region where the plasma flow can have a component in the direction of a density gradient. In this region, the gradient drift instability develops [e.g., *Tsunoda*, 1988], and high backscatter power signal would be observed from this part [e.g., *Milan et al.*, 2002]. The high backscatter power region is an interface between the preexisting flow generally in the antisunward direction and the B_Y-associated fast zonal flow. The dotted region immediately poleward of the reconnection line represents the density gradient produced by the cusp particle precipitation. Fine structure within the cusp precipitation can produce a density gradient in the direction of the flow [e.g., *Moen et al.*, 2002]. The structured contour near 0900 MLT in Figure 9 reflects this situation.

[42] Subsequent increase in IMF $|B_Y/B_Z|$ together with the decrease in negative B_Z would cause the poleward shift of the cusp, and expands the zonal flow region smoothly toward the postnoon side. The density gradient region also continues to drift in the poleward and eastward direction. This is the poleward moving feature of the radar backscatter.

[43] The dawnward shifted portion of the reconnection line is presumably located in the off-equatorial plane of the magnetopause or on the southern side of the equatorial plane because of tilted reconnection line [e.g., *Nishida and*

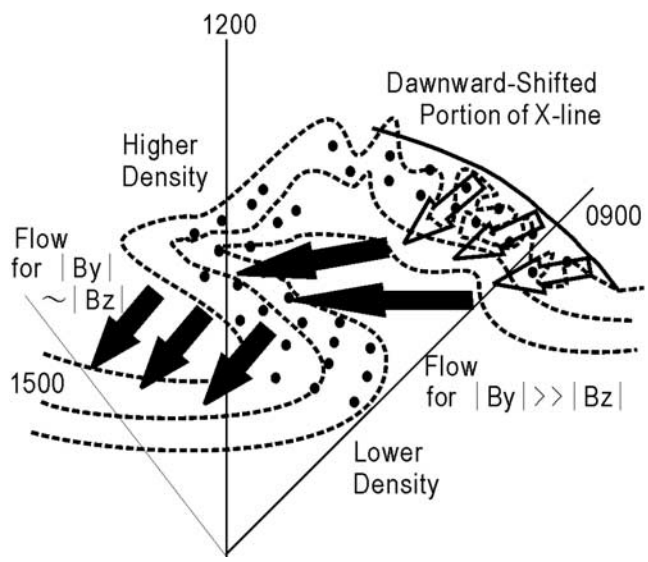

Figure 9. Schematic illustration of the inferred plasma density profile and the flow pattern at time of polar patch formation. The density profile (shown with dashed contours) represents that the tongue of ionization that was created before polar patch formation is about to be broken into a patch. Faster flow (longer bold arrows) appears in response to IMF $|B_Y| \gg |B_Z|$, and breaks the tongue of ionization. The shorter bold arrow indicates the flow inside the patch. Solid dots represent the region where the plasma flow can have a component in the direction of the density gradient.

Maezawa, 1971; *Mozer et al.*, 1974]. The tension force acting on the northern reconnected flux tubes has a downstream component, which does not compete with the sheath flow. In the northern prenoon ionosphere, the flow would be more or less antisunward (reddish color region in the second row in Figure 7). These northern (or southern) flux tubes eventually form a low-latitude mantle in the dawnside (or duskside) flank in the near-Earth magnetotail [*Taguchi et al.*, 2001; *Kishida et al.*, 2002].

[44] On the postnoon side in the northern ionosphere, the westward flow region expands toward the prenoon side. This explains the correlation between the poleward motion of the LENA cusp and the longitudinal motion of the boundary between the sunward flow and antisunward flow regions which has been identified in the Hankasalmi radar. Our interpretation suggests that the polar patch should exist at higher latitudes in the northern ionosphere because a mirror image is assumed. However, we cannot confirm this because the two radars in the northern hemisphere do not receive any significant backscatter echoes from ~80° MLAT. Backscatter echoes are detected when two critical requirements are satisfied: field-aligned irregularities must be present within the FOV, and the ionospheric propagation conditions must be such that HF waves can reach the ionosphere at a substantial distance from the radar site.

4.2. Test for Two Mechanisms for the Less Dense Plasma Behind the Patch

[45] For the less dense plasma associated with the fast flow, two mechanisms have been proposed. One is plasma depletion, which has been proposed by *Valladares et al.* [1994] and *Rodger et al.* [1994]. The fast plasma flow can cause a rapid depletion of ionization because of the increased $O^+ + N_2$ reaction rate associated with ion-neutral frictional heating [*Schunk et al.*, 1975]. Another mechanism is the rapid transport of less dense plasma from other MLTs [e.g.,*Valladares et al.*, 1996; *Lockwood et al.*, 2000].

[46] In our event, the initial signatures that can be associated with less dense plasma behind the patch are the appearance of the zonal flow (at the Kerguelen radar) and the low backscatter power region at 76°–78° in 1000–1100 MLT (at the Syowa radar). Since the zonal flow is on the reconnected open field lines, it must come through the footprint of the reconnection line located at ~72° (Figure 8b).

[47] For simplicity, we consider a situation in which plasmas come to 77° in 1000 MLT from the middle point between C and D on the reconnection line. The distance of this path is about 600 km. Previous studies have shown that the flow speed at the cusp during large IMF B_Y can be ~4 km s^{-1} [e.g., *Maynard et al.*, 1991; *Wilson and Craven*, 1999; *Bosqued et al.*, 2005]. When we take the initial speed to be 2 km s^{-1}, and assume that the speed linearly increases along the path and reaches 3 km s^{-1} or 4 km s^{-1} at the destination, it requires ~4 or ~3.5 min for the plasmas to get there. Since the zonal flow can be seen at 0840 UT (Figure 8b), these elapse times imply that the initial signature should be seen at 0836–0837 UT. The Pykkvibaer radar data show that the zonal flow component starts to increase at such times (Figure 6b). Hence, a rapid depletion of the ionization caused by the frictional heating fits in the present observation.

[48] The present study based on the radar data does not provide any direct evidence for how much the plasma is depleted. However, previous modeling studies suggest that the assumed speed of 3–4 km s^{-1} in our event would be fast enough to produce a depletion of the ionization. *Schunk et al.* [1975] have shown that the electron density around the altitude of ~300 km is reduced by a factor of about 1.5 when the electric field increases from 100 mV/m (flow speed of ~2 km/s) to 200 mV/m (flow speed of ~4 km/s). *Balmforth et al.* [1999] have reached a similar conclusion for the velocity enhancement of 2.5 km s^{-1} which builds up linearly over 100 s.

[49] For the second mechanism mentioned above, *Valladares et al.* [1996] have first pointed out the possible association with the polar patch formation. *Lockwood et al.* [2000, 2005] have proposed a mechanism for polar patch formation during large IMF B_Y by refining the *Lockwood and Carlson* [1992] model, in which the plasma concentration enhancements in the cusp are associated with the pulsed magnetopause reconnection. In this model lower-concentration flux tubes arise from local times further away from the sector in which the polar patch is identified.

[50] In our event, the separation of the polar patch occurs at ~77°. If the low-concentration flux tube comes from lower latitudes, any gap should be seen at lower latitudes in the spatial distribution of the backscatter power. However, there are no such signatures in the data before the time of the polar patch formation. If we consider the possibility that the low-concentration flux tube is "hidden" around 72° near the cusp immediately before the polar patch identification, and then reaches 77°, the flux tube should move at least along the distance of 5° (=77°–72°) within 1 min, i.e., the data resolution of the radar data in this event. This needs a drift speed of ~9 km s^{-1}, which is rather unusual in the polar ionosphere. The transport of the lower-concentration flux tube from earlier MLTs would require more unusual drift speed. This mechanism would not explain polar patch formation in this event.

4.3. Comparison With Previous Studies

[51] The coincidence of the formation of a polar patch with such a rapid flow has been pointed out by *Pinnock et al.* [1991]. Further evidence has been provided by *Rodger et al.* [1994], who have suggested the significance of the density depletion caused by the rapid flow, and the rapid change of IMF B_Y. *Rodger et al.* [1994] have also suggested that $B_Y \sim 0$ is necessary for the interpretation of the poleward moving signatures of the polar patch. *Milan et al.* [2002] have suggested that the change in B_Y polarity is partially responsible for modulating the patch formation, in much the same way that was proposed by *Rodger et al.* [1994]. In our interpretation, $B_Y \sim 0$, i.e., southward IMF after the appearance of the zonal flow is not needed. Southward IMF is required as a preexisting condition (before polar patch formation). Regarding Figure 5 of the *Rodger et al.* [1994] paper, we note that the IMF B_Y magnitude increases sharply after $B_Y \sim 0$, i.e., $|B_Y/B_Z|$ increases, which is consistent with our event.

[52] *Sojka et al.* [1993] have shown in their simulation that repetitive changes in the polarity of IMF B_Y can lead to the production of large-scale plasma structures by redirecting the tongue of ionization toward different locations in the

polar cap. These suggestions cannot explain our event because there is no change of the IMF B_Y sign (Figure 4). In terms of the importance of the time-varying convection, however, the result by *Sojka et al.* [1993] is consistent with our interpretation. In our interpretation the rapid flow must turn on, which means that the time varying convection is required for patch formation.

[53] Although the transport of less-ionized plasmas from earlier MLTs is not a dominant mechanism for this event, it should be pointed out that the density of the plasmas brought by the B_Y-controlled zonal flow into the polar cap is not as high as the one brought by the flow near noon sector during purely southward IMF. This situation should make the density depletion structure clearer for an IMF B_Y-dominated period. For purely southward IMF, the frictional heating may be also caused by the fast antisunward flow, but a depletion of ionization would not be prominent because increasing higher density plasma can be brought in that region.

5. Conclusions

[54] The LENA signal, as a tool of monitoring the cusp, provides the latitude of the footprint of the reconnection line, i.e., the boundary of the open and closed field lines in the ionosphere. The consistency of this location and motion with the convection change observed with the SuperDARN radar has clarified the characteristics of the formation of the large-scale polar patch observed on 28 March 2001. The separation of the polar patch occurs at $\sim 5°$ higher latitudes than the footprint of the reconnection line. Immediately before the patch formation, this footprint starts to move poleward. We interpret these observations, including features obtained with other SuperDARN radars in the northern hemisphere, as being due to the IMF B_Y-controlled zonal jet flow that occurred during a period of increase in $|B_Y/B_Z|$. The sharp equatorward boundary of the radar signatures of the polar patch would be an interface between the preexisting flow generally in the antisunward direction and the faster zonal flow. The flow enhancement appears to be a fundamental process that forms the large-scale polar patch at latitudes several degrees higher than the cusp and to cause less dense plasmas behind the patch by a depletion of the ionization because of chemical reaction that is associated with ion-neutral frictional heating.

[55] **Acknowledgments.** This research was supported by Grant-in-Aid for Scientific Research (C) 18540443 under Japan Society for the Promotion of Science and by the IMAGE Project under UPN 370-28-20 at Goddard Space Flight Center. The authors would like to acknowledge valuable discussion with Yozo Murata and Shin Suzuki. The authors are indebted to the PIs of the various SuperDARN radars, without whose efforts this study would not have been possible. The 41th Japanese Antarctic Research Expedition (JARE) has carried out the HF radar operation at Syowa station. CUTLASS (Hankasalmi and Pykkvybaer radar pair) is supported by an award from STFC. The authors also thank C. T. Russell (PI of Polar magnetic field data), D. McComas (PI of ACE plasma data), N. Ness (PI of ACE magnetic field data), J. H. King, and N. Papatashvilli (OMNI data) for providing data through the NASA CDAWeb.

[56] Amitava Bhattacharjee thanks Nozomu Nishitani and another reviewer for their assistance in evaluating this paper.

References

Anderson, D. N., J. Buchau, and R. A. Heelis (1988), Origin of density enhancements in the winter polar cap ionosphere, *Radio Sci.*, *23*, 513–519, doi:10.1029/RS023i004p00513.

Araki, T., T. Kamei, and T. Iyemori (1984), Polar cap vertical currents associated with northward interplanetary magnetic field, *Geophys. Res. Lett.*, *11*, 23–26, doi:10.1029/GL011i001p00023.

Baker, K. B., J. R. Dudeney, J. R. Greenwald, M. Pinnock, P. T. Newell, A. S. Rodger, N. Mattin, and C.-I. Meng (1995), HF radar signatures of the cusp and the low-latitude boundary layer, *J. Geophys. Res.*, *100*, 7671–7695, doi:10.1029/94JA01481.

Balmforth, H. F., R. J. Moffett, and A. S. Rodger (1999), Localized structure in the cusp and high-latitude ionosphere: A modeling study, *Ann. Geophys.*, *17*, 455–462, doi:10.1007/s00585-999-0455-0.

Basinska, E., W. Burke, N. Maynard, W. Hughes, J. Winningham, and W. Hanson (1992), Small-scale electrodynamics of the cusp with northward interplanetary magnetic field, *J. Geophys. Res.*, *97*, 6369–6379, doi:10.1029/91JA03023.

Bosqued, J. M., et al. (2005), Multipoint observations of transient reconnection signatures in the cusp precipitation: A Cluster-IMAGE detailed case study, *J. Geophys. Res.*, *110*, A03219, doi:10.1029/2004JA010621.

Buchau, J., B. Reinisch, E. Weber, and J. Moore (1983), Structure and dynamics of the winter polar cap *F* region, *Radio Sci.*, *18*, 995–1010, doi:10.1029/RS018i006p00995.

Burch, J. L. (1973), Rate of erosion of the dayside magnetic flux based on a quantitative study of the dependence of polar cusp latitude on the interplanetary magnetic field, *Radio Sci.*, *8*, 955–961, doi:10.1029/RS008i011p00955.

Burch, J., P. Reiff, R. Spiro, R. Heelis, and S. Fields (1980), Cusp region particle precipitation and ion convection for northward interplanetary magnetic field, *Geophys. Res. Lett.*, *7*, 393–396, doi:10.1029/GL007i005p00393.

Burke, W., M. Kelley, R. Sagalyn, M. Smiddy, and S. Lai (1979), Polar cap electric field structures with a northward interplanetary magnetic field, *Geophys. Res. Lett.*, *6*, 21–24, doi:10.1029/GL006i001p00021.

Collier, M. R., J. A. Slavin, R. P. Lepping, A. Szabo, and K. Ogilvie (1998), Timing accuracy for the simple planar propagation of magnetic field structures in the solar wind, *Geophys. Res. Lett.*, *25*, 2509–2512, doi:10.1029/98GL00735.

Collier, M. R., et al. (2001a), Observations of neutral atoms from the solar wind, *J. Geophys. Res.*, *106*, 24,893–24,906, doi:10.1029/2000JA000382.

Collier, M. R., et al. (2001b), LENA Observations on March 31, 2001: Magnetosheath remote sensing, *Eos. Trans. AGU*, *82*(47), Fall Meet. Suppl., Abstract SM41C-05.

Collier, M. R., et al. (2003), Dust in the wind: The dust geometric cross section at 1 AU based on neutral solar wind observations, in *Solar Wind Ten*, edited by M. Velli, R. Bruno, and F. Malara, *AIP Conf. Proc.*, *679*, 790–793.

Cowley, S. W. H., and W. J. Hughes (1983), Observation of an IMF effect in the Y magnetic field component at geostationary orbit, *Planet. Space Sci.*, *31*, 73, doi:10.1016/0032-0633(83)90032-6.

Cowley, S. W. H., J. P. Morelli, and M. Lockwood (1991), Dependence of convection flows and particle precipitation in the high-latitude dayside ionosphere on the *X* and *Y* components of the interplanetary magnetic field, *J. Geophys. Res.*, *96*, 5557–5564, doi:10.1029/90JA02063.

Crooker, N. U., J. Berchem, and C. T. Russell (1987), Cusp displacement at the magnetopause for large IMF Y component, *J. Geophys. Res.*, *92*, 13,467–13,471, doi:10.1029/JA092iA12p13467.

Escoubet, C. P., M. F. Smith, S. F. Fung, P. C. Anderson, and R. A. Hoffman (1992), Staircase ion signature in the polar cusp: A case study, *Geophys. Res. Lett.*, *19*, 1735–1738, doi:10.1029/92GL01806.

Farrugia, C. J., P. E. Sandholt, N. C. Maynard, R. B. Torbert, and D. M. Ober (2003), Temporal variations in a four-sheet field-aligned current system and associated aurorae as observed during a Polar-ground magnetic conjunction in the midmorning sector, *J. Geophys. Res.*, *108*(A6), 1230, doi:10.1029/2002JA009619.

Fok, M.-C., et al. (2003), Global ENA IMAGE simulations, *Space Sci. Rev.*, *109*, 77–103, doi:10.1023/B:SPAC.0000007514.56380.fd.

Gosling, J. T., M. F. Thomsen, S. J. Bame, and R. C. Elphic (1990), Plasma flow reversals at the dayside magnetopause and the origin of asymmetric polar cap convection, *J. Geophys. Res.*, *95*, 8073–8084, doi:10.1029/JA095iA06p08073.

Greenwald, R. A., et al. (1995), DARN/SuperDARN: A global view of the dynamics of high-latitude convection, *Space Sci. Rev.*, *71*, 761–796, doi:10.1007/BF00751350.

Heelis, R. A. (1984), The effects of interplanetary magnetic field orientation on dayside high-latitude convection, *J. Geophys. Res.*, *89*, 2873–2880, doi:10.1029/JA089iA05p02873.

Heppner, J. P. (1972), Polar-cap electric field distributions related to the interplanetary magnetic field direction, *J. Geophys. Res.*, *77*, 4877–4887, doi:10.1029/JA077i025p04877.

Hosokawa, K., E. E. Woodfield, M. Lester, S. E. Milan, N. Sato, A. S. Yukimatu, and T. Iyemori (2002), Statistical characteristics of Doppler

spectral width as observed by the conjugate SuperDARN radars, *Ann. Geophys.*, *20*, 1213–1223.

Iijima, T., T. Potemra, L. Zanetti, and P. Bythrow (1984), Large-scale Birkeland currents in the dayside polar region during strongly northward IMF: A new Birkeland current system, *J. Geophys. Res.*, *89*(A9), 7441–7452, doi:10.1029/JA089iA09p07441.

Kishida, H., S. Taguchi, T. Mukai, and Y. Saito (2002), Plasma convection in the low-latitude mantle of the Near-Earth magnetosphere, *Adv. Space Res.*, *30*(12), 2781–2786, doi:10.1016/S0273-1177(02)80410-0.

Lockwood, M., and H. C. Carlson (1992), Production of polar cap electron density patches by transient magnetopause reconnection, *Geophys. Res. Lett.*, *19*, 1731–1734, doi:10.1029/92GL01993.

Lockwood, M., and M. F. Smith (1992), The variation of reconnection rate at the dayside magnetopause and cusp ion precipitation, *J. Geophys. Res.*, *97*, 14,841–14,847, doi:10.1029/92JA01261.

Lockwood, M., C. J. Davis, T. G. Onsager, and J. D. Scudder (1998), Modelling signatures of pulsed magnetopause reconnection in cusp ion dispersion signatures seen at middle altitudes, *Geophys. Res. Lett.*, *25*, 591–594, doi:10.1029/98GL00185.

Lockwood, M., I. W. McCrea, S. E. Milan, J. Moen, J. C. Cerisier, and A. Thorolfsson (2000), Plasma structure within poleward-moving cusp/cleft auroral transients: EISCAT Svalbard radar observations and an explanation in terms of large logical time extent of events, *Ann. Geophys.*, *18*, 1027–1042, doi:10.1007/s00585-000-1027-5.

Lockwood, M., J. A. Davies, J. Moen, A. P. van Eyken, K. Oksavik, I. W. McCrea, and M. Lester (2005), Motion of the dayside polar cap boundary during substorm cycles: II. Generation of poleward-moving events and polar cap patches by pulses in the magnetopause reconnection rate, *Ann. Geophys.*, *23*, 3513–3532.

MacDougall, J., and P. T. Jayachandran (2007), Polar patches: Auroral zone precipitation effects, *J. Geophys. Res.*, *112*, A05312, doi:10.1029/2006JA011930.

Matsuoka, A., K. Tsuruda, H. Hayakawa, T. Mukai, and A. Nishida (1996), Electric field structure and ion precipitation in the polar region associated with northward interplanetary magnetic field, *J. Geophys. Res.*, *101*, 10,711–10,736, doi:10.1029/95JA03557.

Maynard, N., T. Aggson, E. Basinska, W. Burke, P. Craven, W. Peterson, M. Sugiura, and D. Weimer (1991), Magnetospheric boundary dynamics: DE 1 and DE 2 observations near the magnetopause and cusp, *J. Geophys. Res.*, *96*, 3505–3522, doi:10.1029/90JA02167.

Mende, S. B., et al. (2000), Far ultraviolet imaging from the IMAGE spacecraft, *Space Sci. Rev.*, *91*, 243, doi:10.1023/A:1005271728567.

Menietti, J. D., and J. L. Burch (1988), Spatial extent of the plasma injection region in the cusp-magnetosheath interface, *J. Geophys. Res.*, *93*, 105, doi:10.1029/JA093iA01p00105.

Milan, S. E., M. Lester, and T. K. Yeoman (2002), HF radar polar patch formation revisited: Summer and winter variations in dayside plasma structuring, *Ann. Geophys.*, *20*, 487–499.

Moen, J., I. K. Walker, L. Kersley, and S. E. Milan (2002), On the generation of cusp HF backscatter irregularities, *J. Geophys. Res.*, *107*(A4), 1044, doi:10.1029/2001JA000111.

Moore, T. E., et al. (2000), The low-energy neutral atom imager for IMAGE, *Space Sci. Rev.*, *91*(1/2), 155–195, doi:10.1023/A:1005211509003.

Moore, T. E., et al. (2003), Heliosphere-geosphere interactions using low energy neutral atom imaging, *Space Sci. Rev.*, *109*, 351–371, doi:10.1023/B:SPAC.0000007524.11258.b4.

Mozer, F., W. Gonzalez, F. Bogott, M. Kelley, and S. Schutz (1974), High-latitude electric fields and the three-dimensional interaction between the interplanetary and terrestrial magnetic fields, *J. Geophys. Res.*, *79*, 56–63, doi:10.1029/JA079i001p00056.

Murata, Y., S. Taguchi, K. Hosokawa, A. Nakao, M. R. Collier, T. E. Moore, N. Sato, H. Yamagishi, and A. S. Yukimatu (2007), Correlative variations of the neutral atom emission in the high-altitude cusp and the low-altitude cusp, *J. Geophys. Res.*, *112*, A11208, doi:10.1029/2007JA012404.

Newell, P. T., and C.-I. Meng (1994), Ionospheric projection of the magnetospheric regions under low and high solar wind pressure conditions, *J. Geophys. Res.*, *99*, 273–286, doi:10.1029/93JA02273.

Newell, P. T., C.-I. Meng, D. G. Sibeck, and R. P. Lepping (1989), Some low-altitude cusp dependencies on interplanetary magnetic field, *J. Geophys. Res.*, *94*, 8921–8927, doi:10.1029/JA094iA07p08921.

Nishida, A., and K. Maezawa (1971), Two basic models of interaction between the solar wind and the magnetosphere, *J. Geophys. Res.*, *76*, 2254–2264, doi:10.1029/JA076i010p02254.

Nishitani, N., T. Ogawa, M. Pinnock, M. P. Freeman, J. R. Dudeney, J.-P. Villain, K. B. Baker, N. Sato, H. Yamagishi, and H. Matsumoto (1999), A very large scale flow burst observed by the SuperDARN radars, *J. Geophys. Res.*, *104*, 22,469–22,486, doi:10.1029/1999JA900241.

Ogawa, T., N. Nishitani, M. Pinnock, N. Sato, H. Yamagishi, and A. S. Yukimatu (1998), Antarctic HF radar observations of irregularities associated with polar patches and auroral blobs: A case study, *J. Geophys. Res.*, *103*, 26,547–26,558, doi:10.1029/98JA02044.

Ogawa, T., S. Buchert, N. Nishitani, N. Sato, and M. Lester (2001), Plasma density suppression process around the cusp revealed by simultaneous CUTLASS and EISCAT Svalbard radar observations, *J. Geophys. Res.*, *106*, 5551–5564, doi:10.1029/2000JA900111.

Oksavik, K., J. M. Ruohomiemi, R. A. Greenwald, J. B. H. Baker, J. Moen, H. C. Carlson, T. K. Yeoman, and M. Lester (2006), Observations of isolated polar cap patches by the European Incoherent Scatter (EISCAT) Svalbard and Super Dual Auroral Radar Network (SuperDARN) Finland radars, *J. Geophys. Res.*, *111*, A05310, doi:10.1029/2005JA011400.

Onsager, T. G., C. A. Kletzing, J. B. Austin, and H. Mackiernan (1993), Model of magnetosheath plasma in the magnesphere-cusp and mantle particles at low-altitudes, *Geophys. Res. Lett.*, *20*, 479–482, doi:10.1029/93GL00596.

Pinnock, M., A. S. Rodger, J. D. Dudeney, R. A. Greenwald, K. B. Baker, and J. M. Ruohoniemi (1991), An ionospheric signature of possible enhanced magnetic field merging on the dayside magnetopause, *J. Atmos. Terr. Phys.*, *53*, 201–212, doi:10.1016/0021-9169(91)90104-F.

Pinnock, M., A. S. Rodger, J. D. Dudeney, K. B. Baker, P. T. Newell, R. A. Greenwald, and M. E. Greenspan (1993), Observations of an enhanced convection channel in the cusp ionosphere, *J. Geophys. Res.*, *98*, 3767–3776, doi:10.1029/92JA01382.

Reiff, P. (1982), Sunward convection in both polar caps, *J. Geophys. Res.*, *87*, 5976–5980, doi:10.1029/JA087iA08p05976.

Reiff, P. H., T. W. Hill, and J. L. Burch (1977), Solar wind plasma injection at the dayside magnetospheric cusp, *J. Geophys. Res.*, *82*, 479–482, doi:10.1029/JA082i004p00479.

Rodger, A. S., and T. J. Rosenberg (1999), Riometer and HF radar signatures of polar patches, *Radio Sci.*, *34*, 501–508, doi:10.1029/1998RS900005.

Rodger, A. S., M. Pinnock, J. R. Dudeney, K. B. Baker, and R. A. Greenwald (1994), A new mechanism for polar patch formation, *J. Geophys. Res.*, *99*, 6425–6436, doi:10.1029/93JA01501.

Roelof, E. C., and A. J. Skinner (2000), Extraction of ion distributions from magnetospheric ENA and EUV images, *Space Sci. Rev.*, *91*, 437–459, doi:10.1023/A:1005281424449.

Russell, C. T., R. C. Snare, J. D. Means, D. Pierce, D. Dearborn, M. Larson, G. Barr, and G. Le (1995), The GGS POLAR magnetic fields investigation, *Space Sci. Rev.*, *71*, 563–582, doi:10.1007/BF00751341.

Schunk, R. W., W. J. Raitt, and P. M. Banks (1975), Effect of electric fields on the daytime high-latitude *E* and *F* regions, *J. Geophys. Res.*, *80*, 3121–3130, doi:10.1029/JA080i022p03121.

Shue, J.-H., et al. (1998), Magnetopause location under extreme solar wind conditions, *J. Geophys. Res.*, *103*, 17,691–17,700, doi:10.1029/98JA01103.

Sojka, J., M. Bowline, R. Schunk, D. Decker, C. Valladares, R. Sheehan, D. Anderson, and R. Heelis (1993), Modeling polar cap *F* region patches using time varying convection, *Geophys. Res. Lett.*, *20*, 1783–1786, doi:10.1029/93GL01347.

Suzuki, S., S. Taguchi, K. Hosokawa, M. R. Collier, T. E. Moore, H. U. Frey, and S. B. Mende (2008), Conjugate observations of ENA signals in the high-altitude cusp and proton auroral spot in the low-altitude cusp with IMAGE spacecraft, *Geophys. Res. Lett.*, *35*, L13103, doi:10.1029/2008GL034543.

Taguchi, S., and R. A. Hoffman (1996), Control parameters for polar ionospheric convection patterns during northward interplanetary magnetic field, *Geophys. Res. Lett.*, *23*, 637–640, doi:10.1029/96GL00452.

Taguchi, S., M. Sugiura, J. D. Winningham, and J. A. Slavin (1993), Characterization of the IMF B_Y-dependent field-aligned currents in the cleft region based on DE 2 observations, *J. Geophys. Res.*, *98*, 1393–1407, doi:10.1029/92JA01014.

Taguchi, S., H. Kishida, T. Mukai, and Y. Saito (2001), Low-latitude plasma mantle in the near-Earth magnetosphere: Geotail observations, *J. Geophys. Res.*, *106*, 1949–1954, doi:10.1029/2000JA900100.

Taguchi, S., M. R. Collier, T. E. Moore, M.-C. Fok, and H. J. Singer (2004a), Response of neutral atom emissions in the low- and high-latitude magnetosheath direction to the magnetopause motion under extreme solar wind conditions, *J. Geophys. Res.*, *109*, A04208, doi:10.1029/2003JA010147.

Taguchi, S., K. Hosokawa, M. R. Collier, T. E. Moore, M.-C. Fok, A. S. Yukimatu, N. Sato, and R. A. Greenwald (2004b), Simultaneous observations of the cusp with IMAGE Low Energy Neutral Atom Imager and SuperDARN radar, *Adv. Polar Upper Atmos. Res.*, *18*, 53–64.

Taguchi, S., S.-H. Chen, M. R. Collier, T. E. Moore, M.-C. Fok, K. Hosokawa, and A. Nakao (2005), Monitoring the high-altitude cusp with the Low Energy Neutral Atom imager: Simultaneous observations from IMAGE and Polar, *J. Geophys. Res.*, *110*, A12204, doi:10.1029/2005JA011075.

Taguchi, S., K. Hosokawa, A. Nakao, M. R. Collier, T. E. Moore, A. Yamazaki, N. Sato, and A. S. Yukimatu (2006a), Neutral atom emission

in the direction of the high-latitude magnetopause for northward IMF: Simultaneous observations from IMAGE spacecraft and SuperDARN radar, *Geophys. Res. Lett.*, *33*, L03101, doi:10.1029/2005GL025020.

Taguchi, S., K. Hosokawa, Y. Murata, A. Nakao, M. R. Collier, T. E. Moore, N. Sato, and A. S. Yukimatu (2006b), Neutral atom emission coming from the direction of the high-latitude magnetopause under northward IMF, *Adv. Polar Upper Atmos. Res.*, *20*, 17–26.

Trattner, K. J., S. A. Fuselier, S. M. Petrinec, T. K. Yeoman, C. Mouikis, H. Kucharek, and H. Reme (2005), Reconnection sites of spatial cusp structures, *J. Geophys. Res.*, *110*, A04207, doi:10.1029/2004JA010722.

Tsunoda, R. T. (1988), High-latitude *F*-region irregularities: A review and synthesis, *Rev. Geophys.*, *26*, 719–760, doi:10.1029/RG026i004p00719.

Valladares, C. E., S. Basu, J. Buchau, and E. Friis-Christensen (1994), Experimental evidence for the formation and entry patches into the polar cap, *Radio Sci.*, *29*, 167–194, doi:10.1029/93RS01579.

Valladares, C., D. Decker, R. Sheehan, and D. Anderson (1996), Modeling the formation of polar cap patches using large plasma flows, *Radio Sci.*, *31*, 573–593, doi:10.1029/96RS00481.

Valladares, C. E., D. T. Decker, R. Sheehan, D. N. Anderson, T. Bullett, and B. W. Reinisch (1998), Formation of polar cap patches associated with north-to-south ions of the interplanetary magnetic field, *J. Geophys. Res.*, *103*, 14,657–14,670, doi:10.1029/97JA03682.

Weber, E., J. Buchau, J. Moore, J. Sharber, R. Livingston, J. Winningham, and B. Reinisch (1984), F layer ionization patches in the polar cap, *J. Geophys. Res.*, *89*, 1683–1694, doi:10.1029/JA089iA03p01683.

Wilson, G. R., and P. Craven (1999), Molecular ion upflow in the cleft ion fountain, *J. Geophys. Res.*, *104*, 4437–4446, doi:10.1029/1998JA900070.

Yamauchi, M., R. Lundin, and T. A. Potemra (1995), Dynamic response of the cusp morphology to the interplanetary magnetic field changes: An example observed by Viking, *J. Geophys. Res.*, *100*, 7661–7670, doi:10.1029/95JA00333.

M. R. Collier and T. E. Moore, NASA Goddard Space Flight Center, Greenbelt, MD 20771, USA.

K. Hosokawa, A. Nakao, and S. Taguchi, Department of Information and Communication Engineering, University of Electro-Communications, Chofu, Tokyo, 182-8585, Japan. (taguchi@ice.uec.ac.jp)

N. Sato and A. S. Yukimatu, National Institute of Polar Research, Tokyo, 173-8515, Japan.